Shaking assisted self-assembly of rectangular-shaped parts

Dung-An Wang and Ben Liao

Institute of Precision Engineering, National Chung Hsing University, 250 Kuo Kuang Rd, Taichung 402, Taiwan, Repubic of China

E-mail: daw@dragon.nchu.edu.tw

April 20, 2009

Abstract

A process for shaking assisted self-assembly of rectangular-shaped parts is presented. Rectangular parts are assembled to their corresponding binding sites on a glass substrate in an air environment. Rectangular binding sites are the only hydrophilic areas on the substrate. By a dip-coating process, molten solders wet only the binding sites on the substrate. The parts with misalignment angle up to 90° can be rotated and translated to align with the binding sites during orbital shaking. Before the shaking, the solder is reflowed by heating to 120° C. The alignment completed within 3 seconds. The yields of the self-assembly for misalignment angles ranging from 15° to 90° are at least 80%. The integrity of the bonding between the parts and the binding sites is confirmed by a static debonding test.

Keywords: self-assembly; shaking; molten solder; alignment

1. Introduction

It is a major challenge to develop micro and meso scale assembly methods for discrete components in complex heterogeneous integrated systems. Assembly of microparts has been done by the conventional pick and place robotic assembly (Mølhave et al., 2004), microstructure transfer between aligned wafers (Holmes and Saidam, 1998; Singh et al., 1999), and dynamic self-assembly (Grzybowski et al., 2004). Mølhave et al. (2004) demonstrated that micro tweezers can pick up nanowires and an electron beam deposition of carbon residues can be used to assemble nanotubes. Success of their pick-and-place assembly requires a careful design of the shape of the tweezers and precise control of the gripping force. Pick-and-place assembly is a serial process and can be subject to adhesion forces resulting from handling and positioning micro/nano components. Another limitation of the pick-and-place assembly is its inefficiency with large number of components. Holmes and Saidam (1998) performed a wafer-scale assembly of hybrid devices. Their method is applicable to devices which can be assembled by adding components from one direction only. Singh et al. (1999) achieved wafer-level transfer and assembly of microstructures using break-away tethers and solders. Wafer-level transfer is an inherently two-dimensional fabrication method and cannot generate truly three-dimensional structures (Saeedi et al., 2006). Self-assembly where micro-fabricated components are integrated and constructed automatically as functional units is suitable for the development of complex microsystems and because it requires that the target structures be the thermodynamically most stable ones open to the system, it tends to produce structures that are relatively defect-free and self-healing (Whitesides, 1996).

Parts assembled by self-assembly need a method for the mechanical connection to hold the final structure together and electrical connection between components to make the final assembled structure functional. Different ways can be applied to make the electrical connection between components. Solders applied by electroplating, screen printing or sputtering can produce reliable electrical connection for wafer to wafer bonding (Sparks et al., 2001). However, the electrical contacts produced by electroplated solders suffer from poor mechanical properties (Xiong et al., 2003). Polymer interconnections show great promise as conducting materials in a wide range of application areas due to their tolerance of mechanical stress, ease of processing and their chemical tunability (Videlot et al., 2004). Nevertheless, their electrical resistivity is high, their contact area may be limited to asperities, and at the molecular level they may not be able to withstand high-temperature processing and operation (McCreery, 2004; Saeedi et al., 2006). Soldering processes for assembly of parts to each other or to a substrate can provide excellent electrical, thermal, and mechanical properties.

Methods of assembling parts using molten solder have been developed with different driving mechanisms (Harsh et al., 1999; Jacobs et al., 2002; Greiner et al., 2002; Lienemann et al., 2003; Stauth and Parviz, 2005; Ye et al., 2006; Fang et al., 2006; Liu et al., 2007; Morris and Parviz, 2008). Based on surface energy minimization of molten solder balls, Harsh et al. (1999) demonstrated an assembly of a hinged plate through control of solder volume. Jacobs et al. (2002) showed a patterned assembly of LEDs involving liquid solder. The components were suspended in water and agitated gently. Minimization of the free energy of the solder-water interface provided the driving force for the assembly. Their experiments were performed in water in order to reduce capillary and gravitational forces. Greiner et al. (2002) coated the microparts and the on-substrate binding sites with a self-assembled monolayer (SAM), and applied a lubricant liquid to the binding sites while the entire system was immersed in water. They showed that the microparts were attracted to the lubricant sitting on the binding sites due to capillary forces. Lienemann et al. (2003) described a technique of self-assembling microparts onto Au binding sites patterned on a substrate. A SAM layer was adsorbed on the Au binding sites, and a lubricant was applied onto the binding sites. In their assembly process, the microparts were attracted to the binding sites in a water environment with agitation. Stauth and Parviz (2005) performed a fluidic self-assembly of microfabricated silicon components on a flexible, plastic substrate. Their self-assembly was driven by a combination of gravity, capillary forces and dynamic fluid flow. Liu et al. (2007) demonstrated a fluid self-assembly method, which is able to integrate micro components in a multi-batch-wise manner. They patterned solders with different melting points, and activated them separately and sequentially to achieve programmable self-assembly of micro components. A magnetic field was employed by Ye et al. (2006) to integrate nanowires with a solder-padded substrate. A few drops of a suspension of the nanowires in ethanol were placed on top of the substrate in a vial. The vial was then agitated during assembly. Morris and Parviz (2008) assembled circular and square micropart to the binding sites on a silicon template in a fluid environment. In most self-assembly processes, effective part-to-substrate assembly were achieved in fluid environments. Mild fluid self-assembly conditions (temp $<100^{\circ}\mathrm{C}$, $\mathrm{pH} \approx 3.5$) are required for most electronics and photonics components (Stauth and Parviz, 2005).

Without immersing micro components in fluid, Fang et al. (2006) demonstrated an orbital shaking assisted self assembly of square PZT parts in an air environment.

In this paper, a simple process to achieve on-substrate self-assembly of rectangular parts using molten solder is reported. The assembly technique is assisted by an external shaking and provides accurate placement of parts in an air environment. Fabrication steps for the parts and binding sites are described. Experiments for parts with various misalignment angles and shift distances are carried out. Bonding strength between parts and binding sites is investigated by a debonding test.

2. Shaking assisted self-assembly

Surface tension has been the driving force for the self-assembly technique using molten solder, especially in fluid environment (Scott et al., 2004; Chung et al., 2006). Self-alignment of parts to binding sites via a layer of molten solder occurs due to surface energy minimization of the solder. In practice, most parts are rectangular. The number of minimum energy states depends on the width-to-length ratio of the rectangular parts. Based on calculations of the overlap area carried out by Fang et al. (2006), a square part has four preferred in-plane orientations with rotation angle intervals of 90°, where the surface energy has its local minimums. For micro/nano scale parts, the self-assembly process can be driven by surface tension with fluid agitation (Morris and Parviz, 2008; Chung et al., 2006) or simply through minimization of the interfacial free energy (Chung et al., 2006). With proper agitation in fluid environment, millimeter-sized parts can settle into the orientations with the local minimum surface energy (Xiong et al., 2003; Liu et al., 2007). When assembling millimeter-sized parts in air environment, a means to provide external agitation to assist the assembly process is needed.

To assist self-assembly, orbital shaking can be employed to provide a centrifugal force to the part. The centrifugal force may drag and balance the part on the molten solder so that self-alignment of the part can be achieved through surface energy minimization. Random shaking can also drag and balance the parts on the molten solder, orbital shaking is chosen here for the availability of the experimental apparatus. Fig. 1 illustrates the operation steps of the self-assembly assisted by orbital shaking. Fig. 1(a) shows a misaligned part resting on a binding site. The glass substrate is shaken with the orbital shaker at an angular velocity Ω. This external agitation introduces a centrifugal force F to agitate the part. Then the part is rotated to the states of lower surface energy by surface tension and aligned with the binding site as shown in Fig. 1(b).

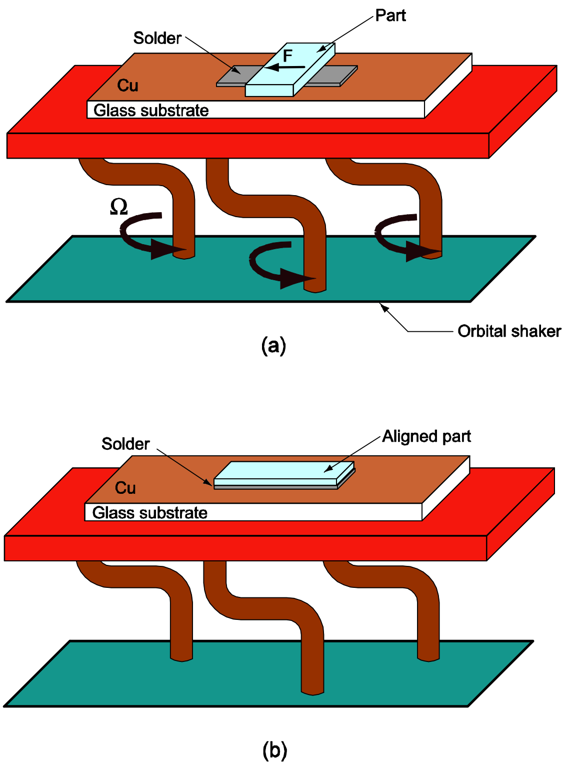

Fig. 1 Two-step operation of the self-assembly of a part. (a) The shaking of an orbital shaker. (b) The resulting alignment of the part.

2.1 Model

Successful alignment of the part to the binding site requires that the magnitude of the centrifugal force F is less than the restoring force T induced by the surface energy minimization. The centrifugal force is given as

$$F = mR\Omega^2 \tag{1}$$

where m is the mass of the part and R is the rotating arm length of the orbital shaker. Using Eq. (1) and the fact that $F < T$ for successful alignment, the angular velocity of the orbital shaker has an upper limit $\Omega_{\max}$

$$\Omega_{\max} = \sqrt{\frac{T}{mR}} \tag{2}$$

2.2 Estimation of the restoring force

For systems with simple geometry, 2D analytical models have been used to determine the surface force (Lienemann et al., 2003). For systems with complex shapes, numerical simulations can model the 3D surface and nonlinear effects better than 2D analytical models. A freely available software, Surface Evolver (Brakke, 1992; 1999), can be used to obtain the minimal energy surface. Here, we used the software for efficient estimation of the potential energy for various shift distances of the part relative to the binding site. The restoring force T can be computed through a smooth perturbation of the potential energy curve with respect to the shift distance. The following assumptions are made in estimation of the restoring force applied to a part.

- A part residing on molten solder is not tilted.

- A part does not touch the substrate.
- The motion of a part in the direction perpendicular to the substrate is minimal.
- The shape of a part and a binding site is identical.
- Molten solder wets the hydrophilic surfaces of a part and a binding site completely and exclusively.

The surface energy between the solder and the solid surfaces are the input parameters to the software, Surface Evolver, in order to obtain the minimal energy surface. The values of surface energies γ between molten solder and solid surfaces of the part and the binding site are given as (Young, 1805)

$$\gamma_{Si} = \gamma_{iA} - \gamma_{SA} \cos\phi \tag{3}$$

where γ_{Si} is the interfacial energy between solder and solid surface i. γ_{iA} is the surface energy between solid surface i and air environment. ϕ is the contact angle between molten solder and the solid surfaces. In this investigation, solder, part, binding site and air environment are denoted by S, P, B and A, respectively. The value of γ_{SA} can be measured by a goniometer.

Fig. 2(a) shows an initial solder shape input to Surface Evolver, for the part orientation angle θ of 90°. Surface Evolver can evolve the initial shape toward a minimum energy profile. Given the device constraints (volume and density of the solder, mass of the part, wetted areas, and gravity), the initial shape does not need to closely approximate the final shape as long as the constraints are set appropriately (Harsh et al., 1999). Fig. 2(b) shows the surface that has been evolved several iterations to a lower potential energy shape. The final energy-minimized shape after evolving for many iterations is shown in Fig. 2(c). The stable shape and corresponding minimum potential energy can be calculated for each shift distance of the part. We can then use the generated potential curve to calculate the restoring force T acting on the part at different shift distances.

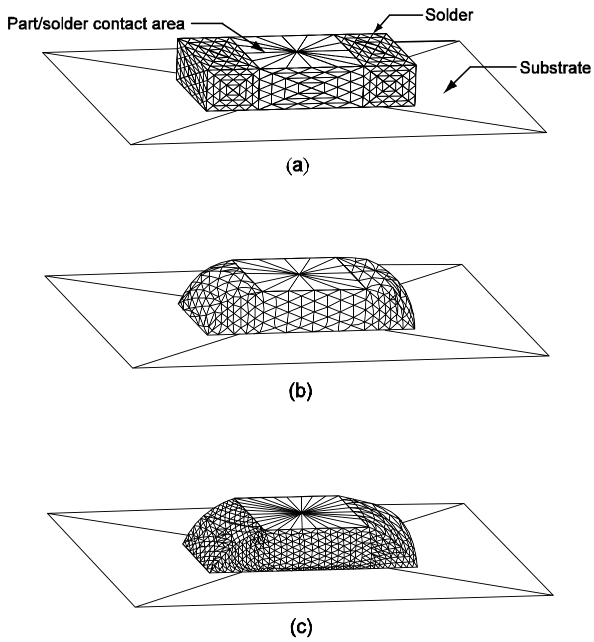

Fig. 2 (a) Initial solder shape input to the Surface Evolver with the orientation angle of a part defined at 90°. (b) Surface that has been evolved several iterations to a lower potential energy shape. (c) Final energy-minimized shape.

2.3 Analysis

The minimal energy surface for various shift distances of the part in the x direction is numerically calculated to predict the restoring force applied to the part by molten solder. Considering the aligned state of the part, the orientation angle θ of the part is 0°. A rectangular part with width $W = 5$ mm, length $L = 10$ mm and thickness $t = 1$ mm is considered. The rectangular shaped binding site has exactly the same lateral dimensions as the part. Molten solder of controlled volume of 0.038 cm^3 wets the binding site. Complete wetting of the binding site is assumed. The value of γ_{SA} used in the numerical investigation is 503 dyne/cm, measured by experiments. The values of surface energy between air and the solid surfaces of nickel and silica are taken as 1850 dyne/cm, γ_{PA}, (Somorjai, 1993) and 300 dyne/cm, γ_{BA}, (Ehrman, 1999), respectively. Using Eq. (3), the values of γ_{SP} and γ_{SB} are calculated as 2206 and 49 dyne/cm, respectively.

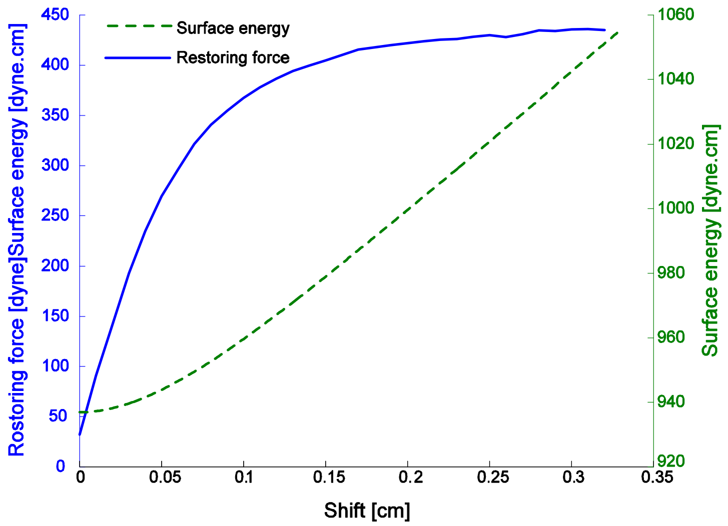

Fig. 3 Surface energy and restoring force as functions of the shift distance.

Fig. 3 plots the surface energy and restoring force as functions of the shift distance of the part from its center of geometry. The surface energy has its minimum at the position of perfect alignment. As the shift distance increases, the surface energy increases and the restoring force first increases linearly and then levels off at a constant value. The restoring force has its maximum value of 436 dyne.

To predict the upper limit of the angular velocity of the orbital shaking, a part with dimensions of 10 x 5 x 1 mm and an orbital shaker with a rotating arm length of 1.5 cm are considered. The mass of the part is 0.37 g. Using Eq. (2) and the maximum value of the restoring force of 436 dyne, the upper limit $\Omega_{\max}$ is calculated as 268 rpm. For the part considered, the angular velocity of the orbital shaker should be properly selected such that the centrifugal force introduced by orbital shaking is less than the restoring force when the part is in perfect alignment with the binding site. The misaligned part with different orientation angles can be driven towards the perfect alignment by surface tension and stay in perfect alignment given the operational angular velocity is less than Ω_{max}. Note that the hydrodynamic and damping effects due to the movement of the part and the molten solder are not considered in the analyses. The analyses presented here serve as a design guideline of the part and orbital shaker used for this self-assembly method.

3. Experiment

3.1 Fabrication of binding sites

The binding site is designed as a rectangular hydrophilic well in a hydrophobic surface. The well is later coated with molten solder. A glass substrate with a binding site is fabricated based on a simple electroforming process. First, a copper foil of 0.5 μm (Yeong-Shin Co., Taiwan) is attached to a glass substrate to form the hydrophobic surface. Next a 5 μm-thick photoresist (AZ4620) is coated and patterned in the binding site region. The Cu layer is patterned by a Cu etchant with H_2O_2/CH_3COOH/water (1:1:18) for 4 hrs to expose the 5 X 10 mm rectangular binding site. Then, the binding site on the glass substrate is etched using a buffered oxide etch solution.

3.2 Surface treatment of parts

5 x 10 x 1 mm rectangular PZT actuators are chosen for demonstration of the self-assembly process in an air environment. The rectangular shape has two preferred in-plane orientations with rotation angle interval of 180°. Compared to square parts which have four preferred in-plane orientations, rectangular parts are good candidates to test the orientation capability of the presented method. PZT actuators are made from PZT powder (Sunnytec, Taiwan) by powder metallurgy and polarized by a lateral poling technique (Cheng et al., 2005). PZT actuators are coated with nickel on one side to render that surface hydrophilic. The nickel coating is implemented using a simple electrodeposition process. First, a PZT actuator is attached to a stainless steel substrate. Next, a 6 μm-thick nickel layer is electrodeposited using a low-stress nickel sulfamate bath with the chemical compositions listed in Table 1. The bath is kept at a temperature of 45 $^\circ C$ and a pH value around 4.0. The current density is 0.075 A/dm^2. Then, the PZT actuators are cleaned with acetone, IPA and DI water in sequence inside a sonicator. Finally, the cleaned parts are dried by baking on a 100 $^\circ C$ hotplate for 5 minutes.

Table 1. Chemical compositions of the low-stress nickel electroplating solution

Chemical	Amount (g/L)
Nickel sulfamate, $Ni(NH_2SO_3)_2 \cdot 4H_2O$	500
Nickel chloride, $NiCl_2 \cdot 6H_2O$	5
Boric acid, H_3BO_3	35
Wetting agent	5

3.3 Dip coating process

Solder is applied on the binding site with a dip coating process. A container for housing the solder is placed onto a hot plate and heated at 120°C until it is melted. A glass substrate with the binding sites is immersd into the molten solder manually. After the substratre is removed from the container, the molten solder only wets the hydrophilic binding sites. Figs. 4(a) and (b) show a patterned substrate before and after the dip coating process, respectively. Fig. 4(a) shows a recessed hydrophilic well in a hydrophobic Cu surface. As shown in Fig. 4(b), after the dip coating, only the hydrophilic binding site is coated with the molten solder.

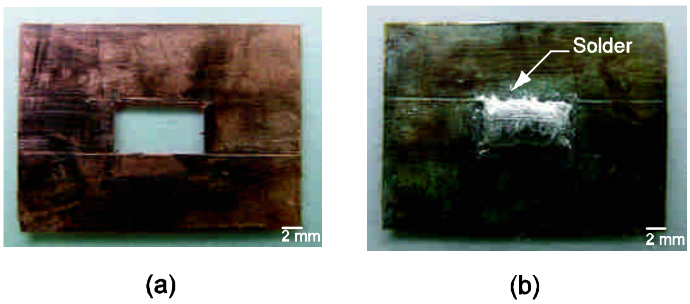

Fig. 4 (a) Patterned Cu layer on a substrate. (b) Only the binding site is coated with molten solder.

3.4 Shaking assisted self-assembly

The self-assembly of the fabricated parts are carried out using the experimental apparatus shown in Fig. 5. A control unit is integrated into the orbital shaker to adjust its angular velocity. The temperature of the heating plate can be set to the desired level by the control unit. A high speed CCD camera mounted on top of an optical microscope is used for capturing the successive images of the self-assembly process. Using computerized frame-by-frame analysis of captured images, the time for alignment of the parts is measured. As shown in the figure, the die containing the device is attached to a heating plate that keeps the solder in molten state. The heating plate is attached onto an orbital shaker (OSR201-01, Genepure Technology, PRC). The rotating arm length of the orbital shaker is 1.5 cm. The upper limit of the angular velocity of the orbital shaker is 300 rpm. The low-temperature solder used in this investigation has a melting point of $72^{\circ}C$.

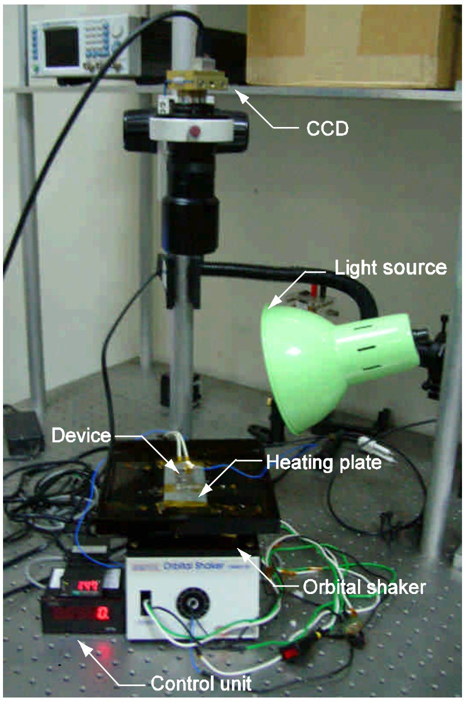

Fig. 5 A photo of the experimental apparatus.

4. Results and discussions

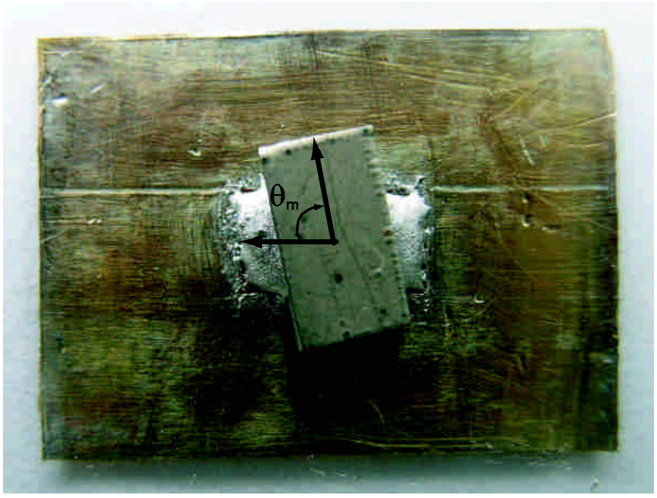

Fig. 6 A rectangular PZT part with a misalignment angle θ_m.

Rectangular PZT parts are selected for demonstration of the self-assembly technique. The length, width, and thickness of the PZT parts are 10, 5 and 1 mm, respectively. The PZT parts are introduced manually without alignment onto the solder with a misalignment angle of θ_m, see Fig. 6. The Ni coated surface of the PZT actuator is facing downward towards the molten solder. By heating the solder on the heating plate with a temperature of $120^\circ C$ and with an external shaking provided by an orbital shaker, the rectangular PZT parts can align with the recessed binding sites. Figs. 7(a) and (b) show a part with a misalignment angle $\theta_m = 80^\circ$ before and after self-assembly, respectively, with the angular velocity $\Omega = 300$ rpm. The alignment between the part and the binding site is excellent as shown in Fig. 7(b).

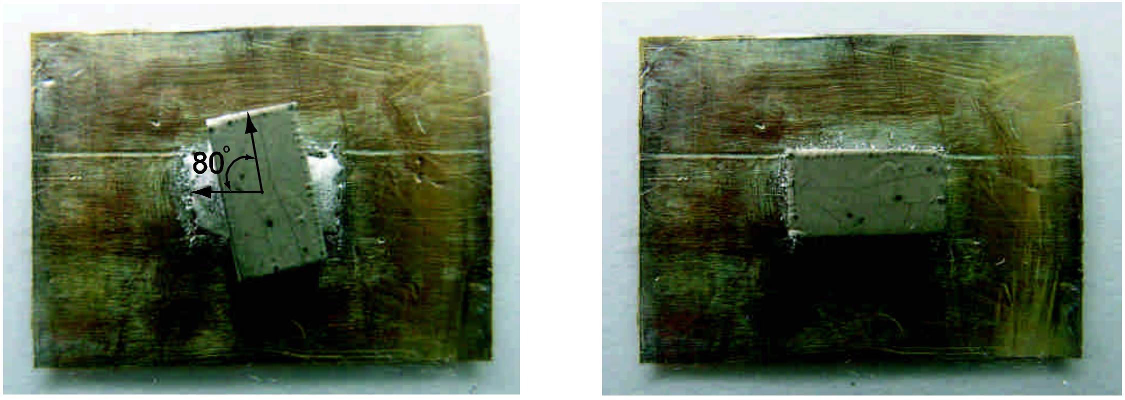

(a) (b)

Fig. 7 A part with a misalignment angle $\theta_m = 80^\circ$ (a) before and (b) after self-assembly.

Based on the experimental observations, the time to alignment for the various tests carried out is less than 3 seconds. Since the alignment took place immediately after the orbital shaker was turned on and ramped up to 300 rpm, the restoring force should be the value for the part at the aligned state. As presented in Section 2.3, the upper limit of the angular velocity for the part considered is 268 rpm, which is close to the experimental result 300 rpm. The 3 X 5 X 0.2 mm nickel parts with misalignment angles of 45° are also successfully aligned to the corresponding binding site. The experiments with 1 X 2 X 0.16 mm nickel parts with misalignment angles of 45° are not successful. The centrifugal force provided by the orbital shaker might not be large enough to drive these parts out of the local minimum energy orientations. Note that the upper limit of the angular velocity of the orbital shaker is 300 rpm. This method can be applied to parts with smaller sizes provided that the centrifugal force applied to the parts is large enough to overcome their local minimum energy wells. Therefore, an orbital shaker with high angular velocities might be needed for alignment of micro parts.

4.1 Effects of misalignment angle

In order to demonstrate the capability of the self-assembly technique, experiments for parts with misalignment angles of 15°, 30°, 45°, 60°, 75° and 90° are carried out at room temperature in an air environment. The angular velocity of the orbital shaker, Ω, is set to be 300 rpm. The temperature of the heating plate is set to be $120^\circ\mathrm{C}$.

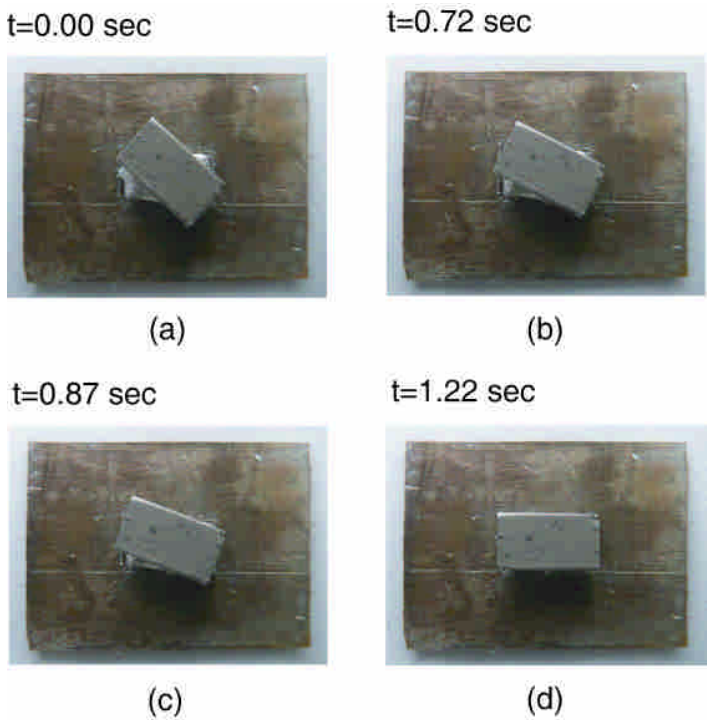

Fig. 8 Snapshots of self-assembly of a part with $\theta_m = 45^\circ$.

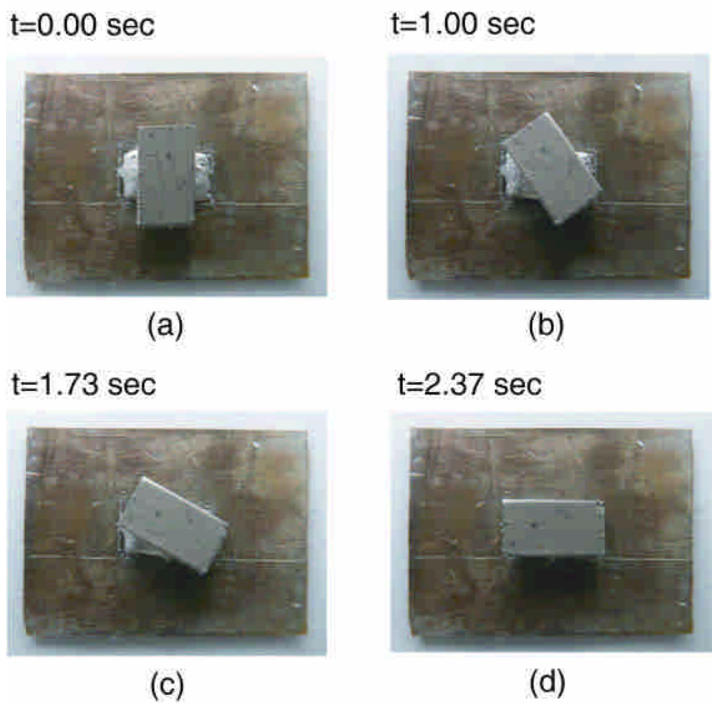

Fig. 9 Snapshots of self-assembly of a part with $\theta_m = 90^\circ$.

Figs. 8 and 9 show sequences of snapshots from experiments for $\theta_m = 45^\circ$ and 90°, respectively. As shown in Fig. 8, a part with $\theta_m = 45^\circ$ is successfully aligned with a binding site within 1.22 sec by orbital shaking. For a part with a large θ_m up to 90°, the self-assembly is completed within 2.37 sec as shown in Fig. 9. It is observed that once alignment between parts and binding sites is achieved, the parts keep aligned with the binding sites during orbital shaking. Fig. 10 shows the alignment time with respect to the misalignment angle. The time for alignment is measured using the frame-by-frame analysis of captured images of the high speed CCD camera. Ten data sets of successful runs are recorded for each misalignment angle. The error bars in Fig. 10 indicate the variation in the experimental results. As shown in Fig. 10, the alignment time increases almost linearly as the misalignment angle θ_m increases. The assembly yield with respect to the misalignment angle is plotted in Fig. 11. The yields of the self-assembly for the six misalignment angles ranging from 15° to 90° are at least 80%. A negative trend of a nearly flat slope in yield is observed as the misalignment angle increases. The effectiveness of the self-assembly technique developed here is confirmed by the high yields observed in the experiments, even for the large misalignment angles.

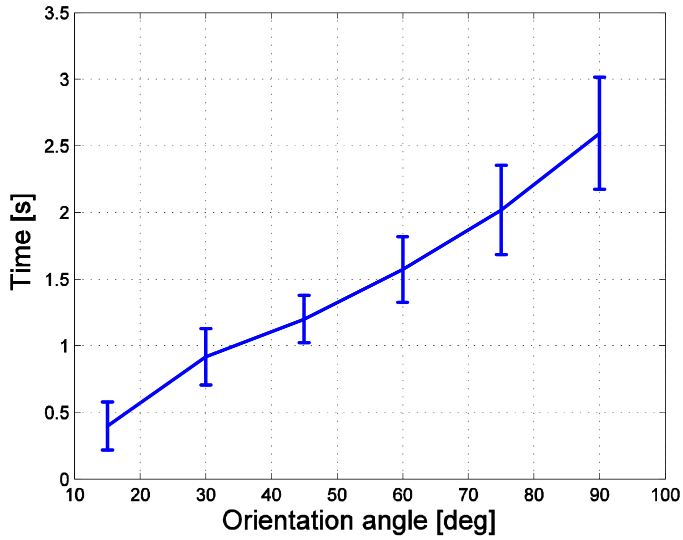

Fig. 10 Alignment time with respect to various misalignment angles.

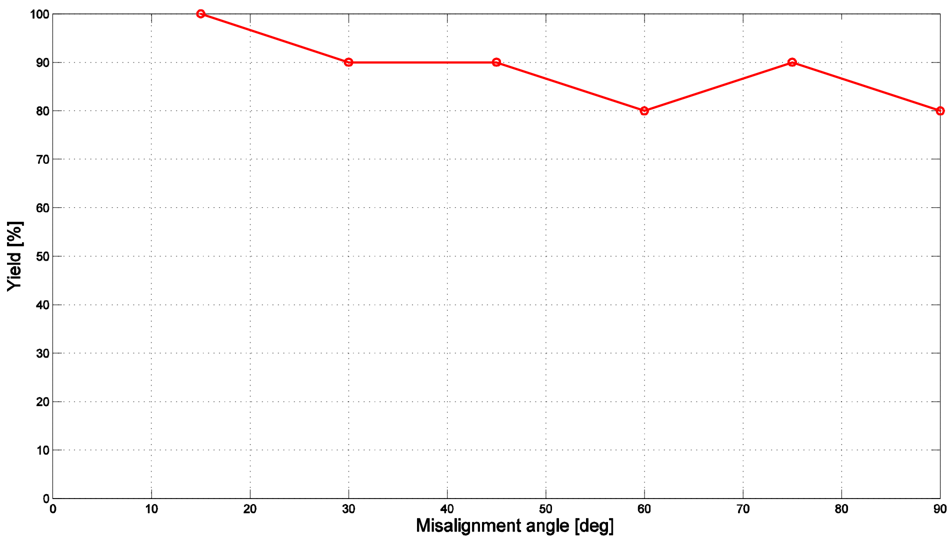

Fig. 11 Alignment yield with respect to various misalignment angles.

4.2 Effects of shift distance

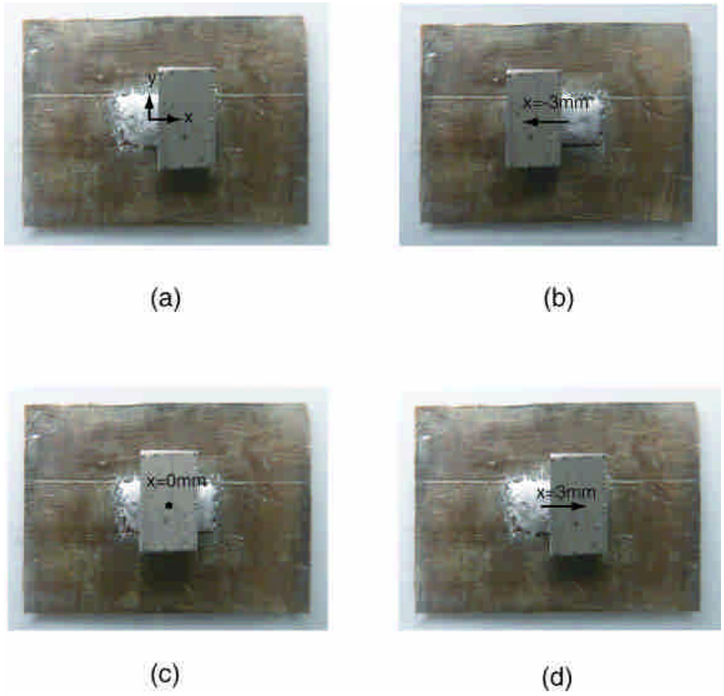

Fig. 12 Photos of parts with different shift distances.

Due to the fact that the parts are manually placed onto the molten solder, the geometry center of the part might not coincide with that of the binding site. In order to understand the effects of the shift distance of parts on the assembly yield, experiments for shifted parts are performed. Fig. 12 shows photos of shifted parts with misalignment angle $\theta_m = 90^\circ$. Fig. 12(a) shows a shifted part and a Cartesian coordinate system. Figs. 12(b), (c) and (d) show parts for the shift displacements of -3, 0, and 3 mm, respectively. The yields for the self-assembly of parts with five shift distances are plotted in Fig. 13. The angular velocity of the orbital shaker is set to 280 rpm in the experiments. For parts with the shift distance of 3 mm, the yields are higher than 50%. As the shift distance increases to 5.5 mm, self-assembly of the parts is not successful. The molten solder on the binding site has a curved surface. Near the edge of the binding site, the curved surface has a larger curvature than the curved surface near the center of the binding site. For the parts with a shift displacement of -5.5 and 5.5 mm, they are tilted significantly. The unsuccessful alignment is attributed to this initial tilting of the part. The unaligned part may tilt and touch the substrate with their corners or edges which prevents the part from rotating toward its perfect alignment.

Experiments carried out in this investigation reveal that no successful run of the self-assembly of the parts is observed when the angular velocity of the orbital shaker is lower than 280 rpm. The unaligned part residing on molten solder tends to tilt and the molten solder may not wet the hydrophilic surfaces of a part and a binding site completely and exclusively. The angular velocity of the orbital shaker should have a lower limit to provide enough centrifugal force to drag the part on the molten solder so that surface tension can drive self-alignment of the part.

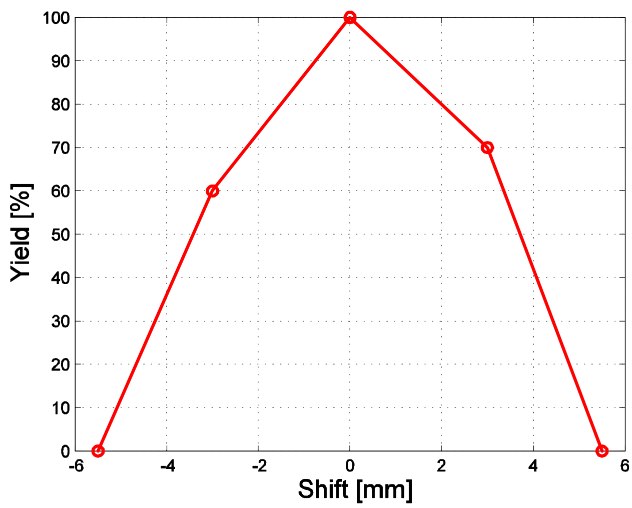

Fig. 13 Alignment yield with respect to various shift distances.

4.3 Wettability of solder

In order to understand the wettability of the solder used in the experiments, contact angles of the molten solder on different surfaces are measured by a FTA200 goniometer (First Ten Angstroms, Inc.) in an air environment. For comparison, contact angles of water on different surfaces are also measured. The pressure and temperature of the droplet ejector are adjusted for contact angle measurements. The droplet ejector is heated to 90°C to melt the solder by a heating coil wrapped around the exterior surface of the ejector. The results, listed in Table 2, indicate that the Ni coated PZT surface is rendered hydrophilic, and the glass surface has much higher attraction than Cu coated glass for water and the molten solder. As demonstrated in the experiments, dipping of the Cu patterned glass substrate in the molten solder leaves the solder only on the glass binding sites.

Table 2. Contact angles of water and molten solder on different surfaces

Surface	Water [deg]	Molten solder [deg]
Cu	80	120
Glass	16	35
Ni	60	70
PZT	85	100

In order to confirm the effective bonding between the part and the binding site, debonding tests are performed. A glass substrate with an aligned part is held vertically by a fixture. The probe tip of a force gauge (FG5020, Lutron Electronic Enterprise Co., Ltd., Taiwan) is pushed against an edge surface of the part. A pressing force applied to the part is increased until the part is debonded, and the final reading of the force gauge is taken as the debonding force. Four rectangular PZT parts assembled are respectively debonded by forces of 25 N, 24 N, 25 N and 24 N. The experimental results indicate that the strength of the bonding is quite uniform. Fang et al. (2006) reported a debonding force of nearly 20 N for their self-assembled square PZT parts. Their PZT parts can actuate pumps with the driving sinusoidal voltage signal as high as 150 kHz.

5. Conclusions

This paper presented a method for an on-substrate self-assembly of rectangular-shaped parts in an air environment. Rectangular parts with a width-to-length ratio of 1:2 are assembled to the corresponding binding sites using molten solder and orbital shaking. Precise alignment of the parts with misalignment angle up to 90° is achieved with a yield up to 80%. The alignment process is completed within 3 seconds. The debonding strength is confirmed by a static debonding test. This assembly technique provides precise placement and high bonding strength of rectangular parts with a high width-to-length ratio by capillary-driven self-assembly. The high-yield self-assembly approach, achieved without precise control of solder volume and complex robotic manipulation, would further shorten production time and lower packaging cost.

Acknowledgement

This work was financially supported by National Science Council, Taiwan (Grant Number: NSC 96-2221-E-005-095). Helpful discussions with K. F. Böhringer of University of Washington are greatly appreciated. The authors would like to express their appreciation to the National Center for High-Performance Computing (NCHC), Taiwan for their assistance.

References

Brakke, K.A., 1992. The surface evolver. Experimental Mathematics 1, 141-165.

Brakke, K.A., 1999. Surface evolver manual, Mathematics Department, Susquehanna University, Selinsgrove, August 18.

Cheng, C.-H., Chen, S.-C., Kuo, H.-C., Chou, Z.-B., 2005. The polling design of a shear mode piezoelectric actuator. J. Micromech. Microeng. 15, 2163-2171.

Chung, J., Zheng, W., Hatch, T.J., Jacobs. H.O., 2006. Programmable reconfigurable self-assembly: parallel heterogeneous integration of chip-scale components on planar and non planar surfaces. Journal of Microelectromechanical Systems 15, 457-464.

Ehrman, S.H., 1999. Effect of particle size on rate of coalescence of silica nanoparticles. Journal of Colloid and Interface Science 213, 258-261.

Fang, J., Wang, K., Böhringer, K.F., 2006. Self-assembly of PZT actuators for micropumps with high process repeatability. Journal of Microelectromechanical Systems 15, 871-878.

Greiner, A., Lienemann, J., Korvink, J.G., Xiong, X., Hanein, Y., Böhringer, K.F., 2002. Capillary forces in micro-fluidic self-assembly. In: Proc. 5th Int. Conf. Modeling and Simulation of Microsystems (MSM ’02), San Juan, Puerto Rico, pp. 198-201.

Grzybowski, B.A., Radkowski, M., Campbell, C.J., Lee, J.N., Whitesides, G.M., 2004. Self-assembling fluidic machines. Applied Physics Letters 84, 1798-1800.

Harsh, K.F., Bright, V.M., Lee, Y.C., 1999. Solder self-assembly for three-dimensional microelectromechanical systems. Sensors and Actuators A 77, 237-244.

Holmes, A.S., Saidam, S.M., 1998. Sacrificial layer process with laser-driven release for batch assembly operations. Journal of Microelectromechanical Systems 7, 416-422.

Jacobs, H.O., Tao, A.R., Schwartz, A., Gracias, D.H., Whitesides, G.M., 2002. Fabrication of a cylindrical display by patterned assembly. Science 296, 323-325.

Lienemann, J., Greiner, A., Korvink, J.G., Xiong, X., Hanein, Y., Böhringer, K.F., 2003. Modelling, simulation and experimentation of a promising new packaging technology – parallel fluidic self-assembly of micro devices. Sensor Update 13, 3-43.

Liu, M., Lau, W.M., Yang, J., 2007. On-demand multi-batch self-assembly of hybrid MEMS by patterning solders of different melting points. J. Micromech. Microeng.

17, 2163-2168.

McCreery, R.L., 2004. Molecular electronic junctions. Chem. Mater. 16, 4477-4496.

Morris, C.J., Parviz, B.A., 2008. Micro-scale metal contacts for capillary force-driven self-assembly. J. Micromech. Microeng. 18, 015022.

Mølhave, K., Hansen, T.M., Madsen, D.N., Bøggild, P., 2004. Towards pick-and-place assembly of nanostructures. Journal of Nanoscience and Nanotechnology 4, 279-282.

Saeedi, E., Abbasi, S., Böhringer, K., Parviz, B.A., 2006. Molten-alloy driven self-assembly for nano and micro scale system integration. Fluid Dynamics & Materials Processing 2, 221-245.

Scott, K.L., Hirano, T., Yang, H., Singh, H., Howe, R.T., Niknejad, A.M., 2004. High-performance inductors using capillary based fluidic self-assembly. Journal of Microelectromechanical Systems 13, 300-309.

Singh, A., Horsley, D.A., Cohn, M.B., Pisano, A.P., Howe, R.T., 1999. Batch transfer of microstructures using flip-chip solder bonding. Journal of Microelectromechanical Systems 8, 27-33.

Somorjai, G.A., 1993. Introduction to chemistry and catalysis. John Wiley & Sons, Inc., New York.

Sparks, D., Queen, G., Weston, R., Woodward, G., Putty, M., Jordan, L., Zarabadi, S., Jayakar, K., 2001. Wafer-to-wafer bonding of nonplanarized MEMS surfaces using solder. J. Micromech. Microeng 11, 630-634.

Stauth, S.A., Parviz, B.A., 2005. Self-assembled silicon networks on plastic. In: Proc. 13th Int. Conf. on Solid State Sensors Actuators (Transducers ’05), Seoul, Korea, pp. 964-967.

Videlot, C., Ackermann, J., Fages, F., Nguyen, T.N., Wang, L., Sarro, P.M., Crawley, D., Nikoli´c, K., Forshaw, M., 2004. Polymer interconnections for 3D-chip stacking technology: directional volume patterning of flexible substrates with conducting polymer wires. J. Micromech. Microeng. 14, 1618-1624.

Whitesides, G.M., 1996. Self-assembly and nanotechnology. In: Proc. SPIE Vol. 2716, Smart Structures and Materials 1996: Smart Materials Technologies and Biomimetics, San Diego, CA, pp. 307-308.

Xiong, X., Hanein, Y., Fang, J., Wang, Y., Wang, W., Daniel, T., Schwartz, D.T., Böhringer, K.F., 2003. Controlled multibatch self-assembly of microdevices. Journal of Microelectromechanical Systems 12, 117-127.

Ye, H., Gu, Z., Yu, T., Gracias, D.H., 2006. Integrating nanowires with substrates using directed assembly and nanoscale soldering. IEEE Transactions on Nanotechnology 5, 62-66.

Young, T., 1805. An essay on the cohesion of fluids. Phil. Trans. R. Soc. Lond. 95, 65-87.